

Transport Induced by Large Scale Convective Structures in a Dipole-Confined Plasma

B. A. Grierson,^{1,*} M. E. Mauel,² M. W. Worstell,² and M. Klassen²

¹Princeton Plasma Physics Laboratory, Princeton University, Princeton, New Jersey 08543, USA

²Department of Applied Physics and Applied Mathematics, Columbia University, New York, New York 10027 USA

(Received 25 November 2009; published 11 November 2010)

Convective structures characterized by $\mathbf{E} \times \mathbf{B}$ motion are observed in a dipole-confined plasma. Particle transport rates are calculated from density dynamics obtained from multipoint measurements and the reconstructed electrostatic potential. The calculated transport rates determined from the large-scale dynamics and local probe measurements agree in magnitude, show intermittency, and indicate that the particle transport is dominated by large-scale convective structures.

DOI: 10.1103/PhysRevLett.105.205004

PACS numbers: 52.35.Mw, 52.35.Ra, 52.55.Hc

The transport of particles, energy, and momentum induced by plasma instabilities determines confinement in magnetic fusion systems. Confinement systems based on a levitated magnetic dipole have been proposed as an alternate path to a fusion reactor due to their relative simplicity and macroscopic stability [1,2]. One key question to be answered about the dipole configuration is whether it has adequate confinement. While drift-resonant transport of energetic particles is understood in dipole geometry [3,4], the transport of thermal plasma confined by a dipole magnet has not been explored in detail. Theoretical and numerical investigations predict the formation of large-scale interchange vortices [5], making plasma transport in the dipole geometry convective. Convective cells have been previously identified in a magnetic trap with a purely toroidal field [6], in a multipole [7], and in a dipole-confined plasma driven by strong rotation [8] or by sustained microwave heating [9].

In this Letter, we report on the first measurement of plasma transport induced by large-scale convective structures in a dipole-confined plasma. An array of 96 retarding-grid particle collectors [10] is biased to image the polar ion current density, and high-speed records of the polar current distribution are used to compute both the instantaneous and time-averaged radial particle flux. We find instantaneous transport occurs in intermittent bursts caused by modulation of density perturbations induced by the time-evolution of the electrostatic potential structure. The large-scale potential appears with closed streamlines that sometimes encircle density perturbations, and cause no transport, and at other times drive bursts of radial transport. Local particle transport measured with Langmuir probes show the same time-averaged flux as the multipoint measurement and also show intermittency, indicating that large-scale convective structures dominate interchange particle transport in a dipole-confined plasma.

We have previously reported observations of the structures of interchange turbulence in a dipole-confined plasma [9]. Turbulent interchange-mode fluctuations are dominated by long wavelength modes with amplitudes which

vary chaotically in time, appear in the lab frame at low-frequencies, $f < 10$ kHz, and have relatively short turbulent correlation times, 50–100 μ s. The potential fluctuations are dominated by two quasiscoherent modes that rotate in the lab frame between 1–2 kHz and have azimuthal mode numbers $m = 1$ and 2. The density perturbations rotate in the same direction as the potential and possess dominant azimuthal modes number up to $m = 4$. Both density and potential perturbations are flute-modes, aligned with a constant phase along magnetic field lines.

All measurements were obtained using the Collisionless Terrella Experiment (CTX) device, described previously [8–10]. Quasisteady turbulent plasma are sustained with electron cyclotron heating (ECRH) of a hydrogen plasma confined by a strong dipole electromagnet that is mechanically supported inside a 1.4 m diameter vacuum vessel. At the poles, the magnetic field strength exceeds 1.5 T, and all fieldlines terminate on insulating surfaces. Figure 1 is a schematic of the experimental apparatus. Plasma density

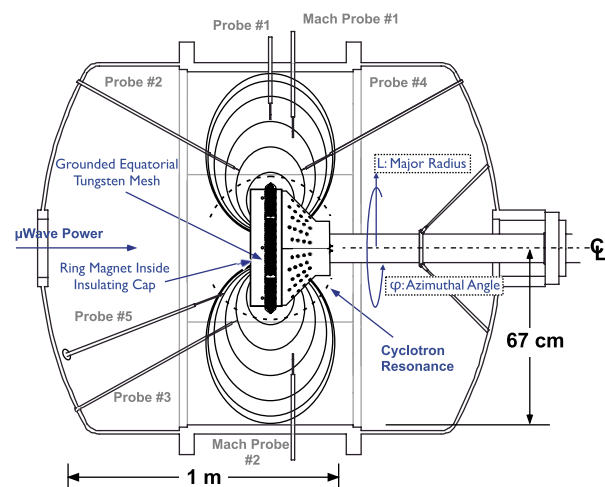


FIG. 1 (color online). The CTX plasma device. Displayed are the magnetic field lines (solid) and ECRH resonance zone (dashed), as well as locations of the movable probes. The polar imager probe array is located at one pole of the electromagnet.

and potential fluctuations are measured locally with movable probes and across the entire plasma confinement region with 96 retarding-grid particle collectors located at one magnetic pole [10]. Data records lasting up to 0.5 s are samples at rates up to 1 Msamples/s. We interpret the ion saturation current to the probes to be proportional to plasma density, and we interpret floating potential fluctuations to be proportional to the electrostatic potential. The ion current collected by each of the retarding-grid detectors of the polar imager is proportional to total ion endloss due to the ion-neutral and ion-ion collision rate. For the discharges reported here, the sum of the ion scattering rates is approximately uniform throughout the plasma so that the polar current is proportional to the number of particles in a flux tube, $N = \langle n \rangle \delta V$, with δV equal to the flux-tube volume linked to the polar detector.

As shown previously [8–10], low-frequency electrostatic potential fluctuations in CTX are constant along a fieldline, $\mathbf{B} \cdot \nabla \Phi = 0$. The electrostatic potential is two-dimensional and parametrized by coordinates that label fieldlines: the magnetic flux, ψ , or the equatorial radius, $L \propto 1/\psi$, and the azimuthal angle, φ . $\Phi(\psi, \varphi, t)$ varies in space from fieldline to fieldline. Measurements show plasma density fluctuations are also two-dimensional. Figure 2 shows the ensemble-averaged cross correlation between one Langmuir probe and a three polar ion current collectors. Although the probe area is more than an order of magnitude smaller than the size of the flux tube measured by the polar collector, we find the local ion saturation current fluctuations are strongly correlated with the flux-tube polar current as expected for interchange motion.

For the conditions reported here, the time-averaged density (as measured by both the polar imager and a movable Langmuir probe) has a radial profile that is slightly steeper than a profile having a uniform N , but less steep than the profile previously used to excite centrifugally driven interchange instabilities [8]. A density profile with $\langle n \rangle \propto 1/\delta V(L) \sim L^{-4}$ [Fig. 3] corresponds to a uniform number of particles in a flux tube, which is the marginal stability profile for rotationally driven interchange modes in a dipole plasma [11], and the stationary profile resulting from turbulent interchange mixing [2,12].

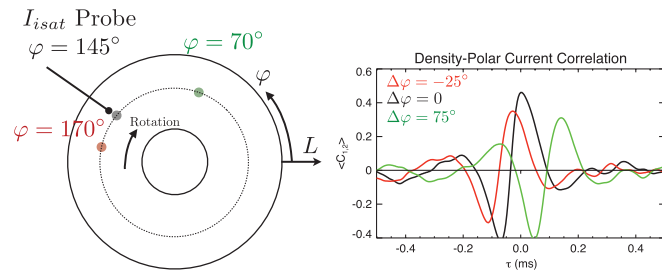


FIG. 2 (color). Experimental configuration and cross-correlation of density measured by a Langmuir probe on the equatorial midplane and polar current. The cross correlation possesses a zero lag time for measurements taken on the same fieldline.

Weak variations from this marginally stable density profile and pressure gradients created from plasma heating excite instabilities that can grow to become large-scale convective cells [5,12,13].

Measurement of large-scale flux-tube convection requires the simultaneous measurement of the plasma ion density and potential structures. Methods have been used to parametrize the outward motion of plasma “blobs” in toroidal devices, and these require either long-time statistics, an identification algorithm to monitor and track blob motion, or optical velocimetry [6,14–21]. The method used for this study is the numerical inversion of the continuity of plasma-filled magnetic flux tubes. High-speed multipoint measurements of the density evolution allows reconstruction of the electrostatic potential structure from the spatial distribution and temporal evolution of the plasma density perturbations. The potential serves as the stream function for plasma interchange motion.

In these discharges, microwaves heat only the electrons, $T_e \gg T_i$, and the plasma beta is relatively low, $\beta \approx 2\mu_0 n T_e / B^2 \sim 10^{-3} \ll 1$. As seen previously [8–10], interchange modes do not create significant parallel currents and magnetic fluctuations do not significant influence $\mathbf{E} \times \mathbf{B}$ flows. The dipole magnetic fieldline geometry, $\mathbf{B} = \nabla\varphi \times \nabla\psi$, defines a coordinate system of magnetic flux ψ and azimuthal angle φ . In this representation, the cross-field flux-tube velocity evaluated at the equatorial plane of the dipole is

$$\mathbf{v} = -L^2 \nabla\varphi \frac{\partial\Phi}{\partial\psi} + \frac{\nabla\psi}{L^2 B^2} \frac{\partial\Phi}{\partial\varphi}. \quad (1)$$

The flux-tube integrated continuity equation is incompressible, and given as

$$\frac{\partial N}{\partial t} - \frac{\partial}{\partial\varphi} \left(N \frac{\partial\Phi}{\partial\psi} \right) + \frac{\partial}{\partial\psi} \left(N \frac{\partial\Phi}{\partial\varphi} \right) = \langle S \rangle. \quad (2)$$

Numerical solutions of Eq. (2) reproduced the kinetic and centrifugal interchange structures and dynamics of

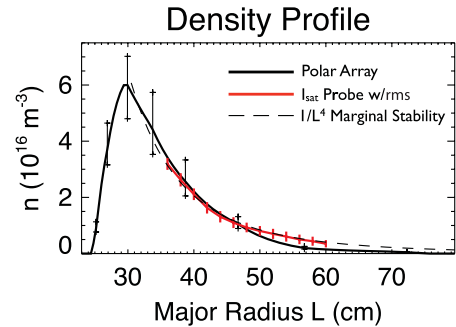


FIG. 3 (color). The density profile measured by the polar imaging array and an internal movable I_{sat} Langmuir probe. The profiles are near marginal stability for interchange modes when $L > L_0$, the ECRH resonance radius at $L_0 \approx 0.3$ m. Vertical bars on the Polar Array and I_{sat} probe display skewed and rms fluctuation amplitudes, respectively.

Refs. [8,10]. The two-dimensional curl of the flux-tube motion is equal to the two-dimensional Laplacian of Φ , which defines the vorticity for the motion of entire flux tubes. The instantaneous radial flux of flux-tube-integrated particle number is expressed as $\Gamma_\psi = \tilde{N} \partial \tilde{\Phi} / \partial \varphi = -\tilde{N} L \tilde{E}_\varphi$, proportional to the azimuthal variation of the electric potential, $L \tilde{E}_\varphi$. The radial motion of plasma flux-tubes is related to the radial flux of particles in geometric coordinates by $\Gamma_r = -\Gamma_\psi / LB \delta V$. Γ_r can be compared to local probe measurements. The term $\langle S \rangle$ on the right-hand side of Eq. (2) embodies the net flux-tube integrated sources and sinks of plasma at their respective spatial and temporal scales.

The polar probe array is distributed evenly in magnetic flux coordinates, simplifying the computation of spatial derivatives. A complete Fourier basis decomposition in flux coordinates is used to expand the time-varying electrostatic potential into spatial harmonics, each with their respective time-varying amplitudes[22]. The potential is represented as $\Phi(\varphi, \psi, t) = \sum_{m,n} \Phi_{m,n}(\varphi, t) \sin(n\pi\psi^*)$, where

$$\Phi_{m,n} = A_{m,n}(t) \sin(m\varphi) + B_{m,n}(t) \cos(m\varphi) + C_n(t) \quad (3)$$

and where $\psi^* = (\psi - \psi_{\min}) / (\psi_{\max} - \psi_{\min})$. The radial variation of the potential was chosen to match the boundary conditions at the magnet of $\Phi(\varphi, \psi_{\max}) = 0$ and at the chamber wall of $\Phi(\varphi, \psi_{\min}) = 0$, which are both grounded. The coefficients $A_{m,n}(t)$ and $B_{m,n}(t)$ contain the azimuthal variation of the potential. These amplitudes (in Volts), are time-varying quantities. The amplitude of the axisymmetric flow pattern is contained in $C_n(t)$, and does not contribute to radial particle flux. By using a finite-difference representation of the density time evolution and spatial derivatives, and substituting the basis function expansion Eq. (3) into Eq. (2), a system of equations for the coefficients $A_{m,n}$, $B_{m,n}$, C_n can be formed and solved in a least-squares sense. The large-scale structure of the electrostatic potential is computed for each time slice in the digitized record.

Figure 4 shows one example of the time evolution of the density and potential structure obtained using the flux-tube velocimetry algorithm. The time evolution shows a large

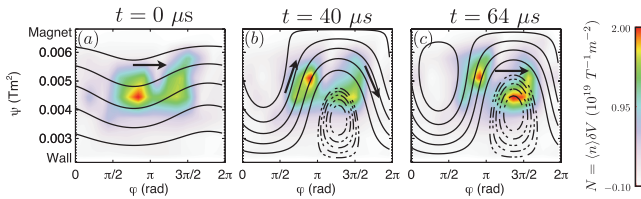


FIG. 4 (color). Motion of plasma density $N(\varphi, \psi, t)$. Solid and dashed lines are negative and positive potential contours, respectively. (a) Azimuthally moving density perturbation. (b) Separation of density perturbation. (c) A convective cell with the density perturbation and potential perturbation with the same azimuthal phase. Arrows indicate direction.

density perturbation rotating azimuthally with initially no closed potential contours. After 40 μs the density structure separates in two, with one part transported into the high flux region and the other part continues to rotate azimuthally. The potential structure at 40 μs begins to develop closed contours around the azimuthally rotating part of the density perturbation, and an open contour on the other part that is transported to the high field region. At 64 μs , the azimuthal phase difference between the density and potential perturbation is near zero. The particle flux calculated for the same time slices is shown in Fig. 5. The radial particle flux agrees with the observed motion of the density perturbation. An important observation is that the radial flux is intermittent on the time scale of one azimuthal rotation of the structure around the device. In Fig. 5(c), we show the computed flux at 64 μs . The flux at this time instant is much reduced compared to the flux at 40 μs . When the potential contour is approximately centered about the density perturbation, an eddy is formed which exhibits particle circulation with little net radial particle transport. The observation of intermittency in the amplitude of the radial particle transport is consistent with the chaotic nature of the fluctuations [9]; indeed the illustrated dynamics in Figs. 4 and 5 are typical and not extraordinary.

The relative phase between density and potential fluctuations determines the magnitude of the transport. A phase shift of $\pi/2$ between the two fluctuating quantities results in maximum radial flux, as seen in Fig. 5(b). When the phase shift is near zero or π , then there is little net transport [Figs. 4(c) and 5(c)].

The simultaneous measurement of density and potential by internal probes on a magnetic fieldline can reveal the sign and magnitude of the local radial particle transport by $\mathbf{E} \times \mathbf{B}$. The observation of convective transport and the intermittency of this transport is consistent with local Langmuir probe measurements. The local radial particle flux, Γ_r , measured by a potential probe and Langmuir probe at $L = 60$ cm and on the same magnetic fieldline in the plasma provides a local measurement of the radial particle flux [23]. With \tilde{n} and $\tilde{\Phi}$ being the fluctuating density and potential, $k_\varphi \sim m/L$ defined as the azimuthal wave number of the potential, $\gamma_{\tilde{n}, \tilde{\Phi}}$ the average coherence, and $\alpha_{\tilde{n}, \tilde{\Phi}}$ the average phase, then $\Gamma_r = \tilde{n} \tilde{v}_r = \tilde{n} \tilde{\Phi} k_\varphi (\gamma_{\tilde{n}, \tilde{\Phi}} / B) \sin \alpha_{\tilde{n}, \tilde{\Phi}}$.

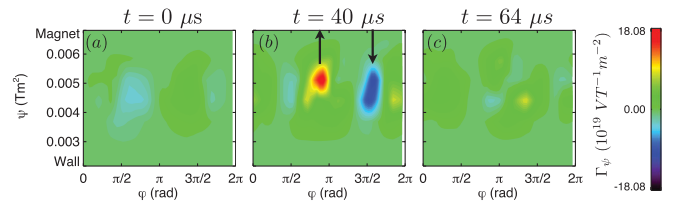


FIG. 5 (color). The radial particle flux associated with Fig. 4. (a) The radial flux for azimuthal propagation at $t = 0$ is low. (b) Burst of inward and outward radial flux, with arrows indicating direction. (c) Reduced flux when the density and potential perturbations have the same azimuthal phase.

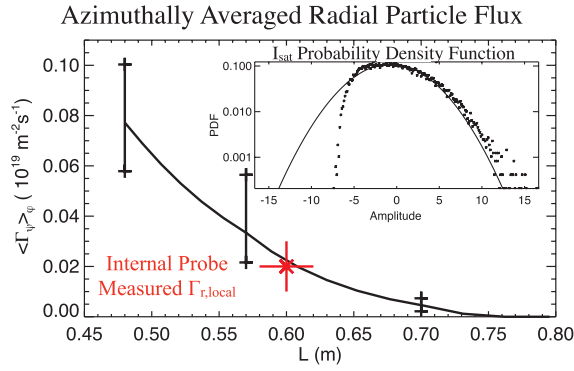


FIG. 6 (color). The time-averaged and azimuthally-averaged radial particle transport rate from both multipoint (black) and local (red) measurement techniques. The locally measured probability density function displays positive skewness indicative of intermittent transport events. Vertical bars on the measurement indicate the fluctuation amplitude, also positively skewed.

Figure 6 compares the time- and azimuthal-angle-averaged radial particle flux calculated by the multipoint reconstruction method with the local particle flux obtained by local probe measurements. Also shown is the probability density function for the density fluctuations displaying intermittency by their skewed-Gaussian character. The local probe measurement gives a time-averaged transport rate of $\Gamma_{r,\text{local}} \approx 1\text{--}3 \times 10^{17} \text{ m}^{-2} \text{ s}^{-1}$ towards the vessel wall. The azimuthally averaged particle flux $\langle \Gamma_{\psi} \rangle_{\phi}$ evaluated at the same radial location agrees with local transport measurements of $\langle \Gamma_{\psi} \rangle_{\phi} / LB \delta V \approx 2 \times 10^{17} \text{ m}^{-2} \text{ s}^{-1}$. While both time-averaged measurements agree numerically, the local measurement does not elucidate the large-scale dynamics by which particles are transported, or indicate whether the particle transport is dominated by small-scale diffusive processes or by large-scale vortex motion.

The time-averaged radial flux is comparable to the quasilinear diffusive flux as described by Ref. [3]. Azimuthal averaging of Eq. (2) gives the quasilinear transport of plasma flux tubes as $\Gamma_{\psi} = -D_{\psi} \partial \langle N \rangle / \partial \psi$, with a quasilinear diffusion coefficient defined in terms of the autocorrelation time, τ_c , of the fluctuating azimuthal electric field, $D_{\psi} = \tau_c L^2 \langle \tilde{E}_{\phi}^2 \rangle$. At $L = 60 \text{ cm}$ the correlation time is $\tau_c \approx 100 \mu\text{s}$ and the rms electric field is $\langle E_{\phi}^2 \rangle \approx 34 \text{ V}^2/\text{m}^2$. The diffusion coefficient is then $D_{\psi} = 0.001\text{--}0.002 \text{ (Vs)}^2/\text{s}$. Since the measurement of the time-averaged density profile is $\langle N \rangle \sim L^{-1/2}$, the quasilinear diffusion of flux tubes agrees with the time average of the measured local particle flux, $\Gamma_r \approx 10^{17} \text{ m}^{-2} \text{ s}^{-1}$.

The measurements described in this Letter identify a confined plasma maintained near marginal stability in the presence of low-frequency interchange turbulence. Measurements of plasma density and potential show the existence of long wavelength convective cells, with radially broad and low-order azimuthal mode numbers, $m = 1$

and 2, with short correlation times. By measuring the density evolution at multiple points across the entire plasma and inverting the flux-tube continuity equation to infer the electrostatic potential, the particle transport associated with the large-scale convective potential structures has been measured for the first time. The particle flux is in good agreement with local measurements obtained by conventional techniques. The instantaneous particle transport is intermittent, and the detailed time evolutions of the perturbed flux-tube number, \tilde{N} , and potential, $\tilde{\Phi}$, indicate that convective transport dominates in the dipole configuration. A key remaining question is whether convective structures will be present and dominate the transport of fusion scale dipole systems [1].

This work was supported by U.S. DOE Grant No. DE-FG02-00ER54585. B. A. G. gratefully acknowledges useful discussions with R. Nazikian, K. H. Burrell, and the LDX team.

*bgriers@pppl.gov

- [1] J. Kesner *et al.*, *Nucl. Fusion* **44**, 193 (2004).
- [2] A. Hasegawa, *Comments Plasma Phys. Controlled Fusion* **11**, 147 (1987).
- [3] T. Birmingham, *J. Geophys. Res.* **74**, 2169 (1969).
- [4] H. Warren *et al.*, *Phys. Plasmas* **3**, 2143 (1996).
- [5] V. Pastukhov and N. Chudin, *Plasma Phys. Rep.* **27**, 907 (2001).
- [6] F. J. Øynes, H. L. Pécseli, and K. Rypdal, *Phys. Rev. Lett.* **75**, 81 (1995).
- [7] G. Navratil, R. Post, and A. Ehrhardt, *Phys. Fluids* **20**, 156 (1977).
- [8] B. Levitt, D. Maslovsky, and M. E. Mael, *Phys. Rev. Lett.* **94**, 175002 (2005).
- [9] B. A. Grierson, M. W. Worstell, and M. Mael, *Phys. Plasmas* **16**, 055902 (2009).
- [10] B. Levitt *et al.*, *Phys. Plasmas* **12**, 055703 (2005).
- [11] D. B. Melrose, *Planet. Space Sci.* **15**, 381 (1967).
- [12] A. Kouznetsov, J. Freidberg, and J. Kesner, *Phys. Plasmas* **14**, 102501 (2007).
- [13] V. Pastukhov and N. Chudin in *Proceedings of the International Atomic Energy Agency 19th Fusion Energy Conference* (IAEA, Lyon, France, 2002) pp. 18.
- [14] T. Munsat and S. Zweben, *Rev. Sci. Instrum.* **77**, 103501 (2006).
- [15] A. Fasoli *et al.*, *Phys. Plasmas* **13**, 055902 (2006).
- [16] I. Furno *et al.*, *Phys. Rev. Lett.* **100**, 055004 (2008).
- [17] O. Grulke, T. Klinger, and A. Piel, *Phys. Plasmas* **6**, 788 (1999).
- [18] O. Grulke *et al.*, *Phys. Plasmas* **8**, 5171 (2001).
- [19] S. H. Müller *et al.*, *Phys. Plasmas* **14**, 110704 (2007).
- [20] S. H. Müller *et al.*, *Phys. Plasmas* **13**, 100701 (2006).
- [21] S. J. Zweben *et al.*, *Phys. Plasmas* **13**, 056114 (2006).
- [22] B. A. Grierson, Ph.D. thesis, Columbia University, 2009.
- [23] M. J. Burin *et al.*, *Phys. Plasmas* **12**, 052320 (2005).